Engineering Structures 316 (2024) 118635

Contents lists available at ScienceDirect

Engineering Structures

journal homepage: www.elsevier.com/locate/engstruct

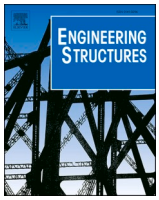

The importance and use of vertical crack displacements for the assessment of existing reinforced concrete deep beams

Alexandru N. Trandafir [a,*], Dhanushka K. Palipana [b], Giorgio T. Proestos [c], Boyan I. Mihaylov [a]

[a] Department of ArGEnCo, University of Liège, Building B52, Quartier Polytech 1, Allée de la Découverte 9, B-4000 Liège, Belgium
[b] Department of Civil, Environmental, Architectural Engineering, University of Kansas, 2155 Learned Hall, 1530 W. 15th St. Lawrence, KS 66045, United States
[c] Department of Civil, Construction and Environmental Engineering, North Carolina State University, 3357 Fitts-Woolard Hall, 915 Partners Way, Raleigh, NC 27695, United States

ARTICLE INFO

Keywords:
Assessment
Cracks
Deep beams
Kinematic model
Residual capacity
Shear

ABSTRACT

The accurate assessment of cracked reinforced concrete structures is becoming increasingly more important as the world's infrastructure ages and resources for retrofit and replacement remain limited. While existing approaches can be used to predict crack information for comparisons with on-site observations, there remains a need to establish methods that use crack measurements as a direct input to assess residual structural capacity. Critical wide cracks have been observed in lightly reinforced deep beams leading to questions about the safety of concrete bridges. To assess such deep members, this paper answers three important questions: 1) which critical crack displacements should be measured?; 2) where should the critical crack displacements be measured?; and 3) what is the residual shear capacity of the member, given the measured critical crack displacements? To answer these questions, detailed data from large-scale experiments is examined and interpreted with the two-parameter kinematic theory (2PKT). The results illustrate the importance of vertical crack displacements for conducting assessments of lightly reinforced deep beams. The paper shows that when the measured crack shape is incorporated into the 2PKT, the residual capacity of deep beams can be determined from measured critical crack displacements.

1. Introduction

As concrete infrastructure ages, the retrofit of bridges, buildings and other critical structures is crucial for maintaining their safety and resilience. At the same time, there are limited resources available to allocate for retrofit; therefore, it has become increasingly more important to enhance structural assessment methodologies used to identify, prioritize, and conduct cost-effective interventions. Cracks in concrete structures are an important visual indicator that can be used for structural assessment. While some current modelling approaches can be used to predict cracks for comparisons with on-site observations, there remains a need to establish methods that use crack measurements as a direct input in the assessment process, referred to here as crack-based assessment methods.

Of particular interest for crack-based assessment are lightly reinforced concrete deep (non-slender) members that can exhibit wide diagonal cracks and brittle shear failures [1]. Such members are commonly found in existing infrastructure in the form of transfer girders in buildings, pier cap beams in bridges, foundations, and thick structural elements in power plants. In recent years, there have been several instances where wide shear cracks have raised questions about the safety of traffic loading on deep pier cap beams in bridge structures [2–4].

To assess the safety of cracked members, Calvi et al. [5] and Zaborac et al. [6] have used measured angles and widths of shear cracks. The observed cracks are approximated as straight and regularly spaced. The crack information is used as an input into a membrane element representing the web of cracked beams, whose behaviour is modelled based on the modified compression field theory [7]. This smeared crack approach may be suitable for slender members with adequate crack control provided by web reinforcement. However, the response of lightly reinforced deep members is governed by a single dominant wide crack, which presents several important challenges. For example, crack widths can vary substantially locally and globally along the crack, and if inappropriate crack measures are used to conduct the assessments, this can lead to variations in the assessment results. Additionally, the exact shape of the critical crack, which is in part determined by random

* Corresponding author.
E-mail address: alexandru.trandafir@uliege.be (A.N. Trandafir).

https://doi.org/10.1016/j.engstruct.2024.118635
Received 6 September 2023; Received in revised form 14 June 2024; Accepted 14 July 2024
Available online 18 July 2024

variations in material and other properties, can have a significant influence on the actual shear strength of the member [1].

To address these challenges, this paper presents a detailed examination of critical shear cracks in lightly reinforced deep members. An analysis is performed using detailed measurements of crack kinematics in a large-scale laboratory test [8,9], as well as based on the modelling framework provided by the two-parameter kinematic theory (2PKT) for deep beams [10]. To conduct crack-based assessments, the paper then answers three key questions:

1) Which critical crack displacements should be measured?
2) Where should the critical crack displacements be measured along the cracks?
3) What is the residual shear capacity of the member, given the measured critical crack displacements?

The study challenges the appropriateness of the use of crack widths, and proposes alternative measurements for crack-based assessment of deep beams. The 2PKT framework is then used to establish a link between the measured critical crack displacement, and the residual shear capacity of cracked members. The measured shape of the shear cracks is directly incorporated in the 2PKT. The obtained residual capacity

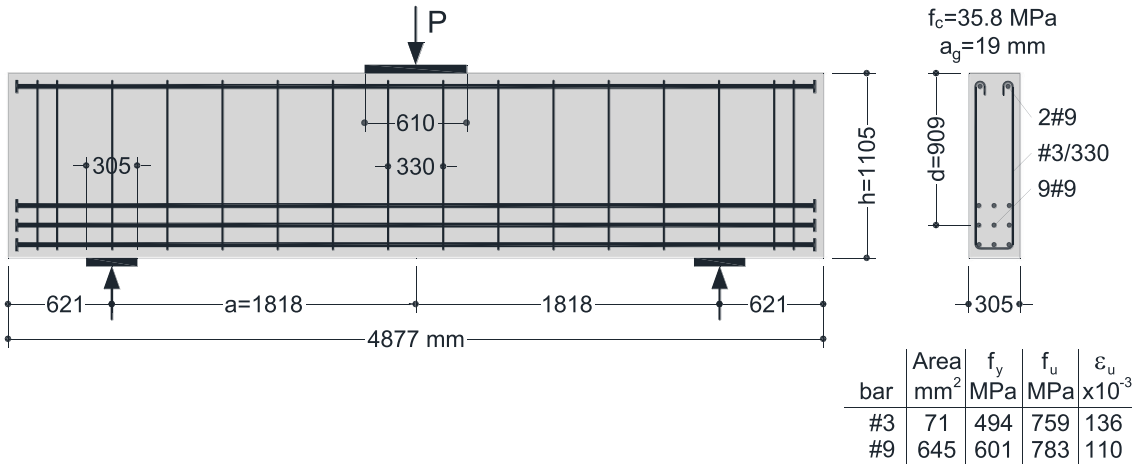

bar	Area mm^2	f_y MPa	f_u MPa	ε_u x10^{-3}
#3	71	494	759	136
#9	645	601	783	110

a) Properties of test specimen CCR2

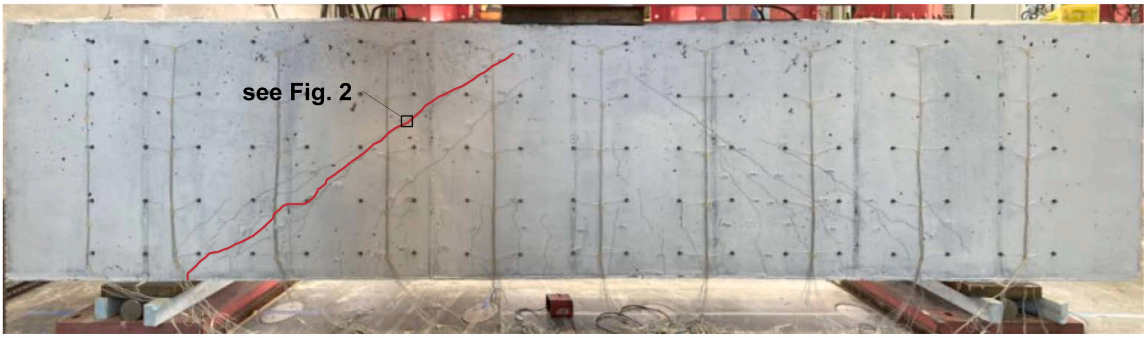

b) Measured crack pattern of test specimen CCR2 at V=0.54V_{max}=600 kN

c) Specimen CCR2 after failure

Fig. 1. Cracking of CCR2 deep beam experiment [8,9].

diagrams are validated with test results from deep beams with various properties and governing shear-carrying mechanisms.

2. Measured crack displacements

2.1. Obtaining crack measurements

Traditionally, site inspections of concrete structures have included the measurement of crack widths. Until recently, crack widths were measured manually with crack comparators or optical devices. Such measurements are typically performed in a limited number of locations and feature significant subjectivity. However, in recent years, the rapid development of various sensing technologies has provided possibilities for advanced crack measurements. In particular, crack shapes and crack widths can now be measured based on high-resolution photographs and image analysis methods [11–14]. This allows for nearly continuous measurements along the entire length of cracks, and also reduces the subjectivity of the results. Furthermore, while manual measurements focus exclusively on crack widths, slip displacements in the cracks can also be extracted from image analysis [15]. Such additional information is important in shear-critical members, where crack slips are associated with aggregate interlock shear stresses across the cracks. Therefore, the availability of advanced technologies for crack measurements raises an important question: Which crack displacements are most useful for the purpose of reliable crack-based assessment of lightly reinforced deep members?

2.2. Experiment of deep beam with detailed crack measurements

To answer this question, it is instructive to examine detailed crack data from an experiment of a deep beam conducted by Palipana and Proestos at the North Carolina State University (specimen CCR2 [8,9]). The beam had a total depth h= 1105 mm and was subjected to symmetrical three-point bending. The geometry and reinforcement of the specimen are shown in Fig. 1a, together with photos of the observed cracks before and after failure. The effective depth of the beam was d= 909 mm and the shear-span-to-depth ratio was a/d= 2.0. The ratio of flexural reinforcement and transverse reinforcement (stirrups) was 2.10 % and 0.141 %, respectively. The compressive strength of the concrete was f_c= 35.8 MPa and the maximum coarse aggregate size was a_g= 19 mm.

The cracking of specimen CCR2 began with flexural cracks at mid-span, followed by inclined flexure-shear cracks in the shear spans. The flexural cracks developed at 10 % of the peak load, while the inclined cracks began to form at 34 % of the peak load. Fig. 1b shows the crack pattern of the beam at 54 % of the peak load, where the flattest inclined cracks extended from the inner edge of the supports to the vicinity of the loading plate (diagonal cracks). As the load increased, the diagonal cracks exhibited opening and slip displacements without significant further crack propagation. As typically observed in deep beams, the failure occurred along a critical diagonal crack with crushing of the concrete in the vicinity of the loading plate (Fig. 1c). The measured shear strength of the beam was V_{max}= 1118 kN. The spalling of concrete visible in Fig. 1c occurred in the post-peak regime.

2.3. Experiment of deep beam with detailed crack measurements

Fig. 1b shows a highlighted portion of the critical crack near mid-depth of specimen CCR2. Fig. 2 shows a close-up photo of this portion of the critical diagonal crack at higher loads (70 % of the peak). It illustrates the crack opening and crack slip that developed at this location. The crack width w is defined as the displacement of one crack surface perpendicular to the opposite surface, while the crack slip s represents the displacement of one crack surface parallel to the opposite surface. From a global perspective, the crack opening is associated with both flexural and shear deformations, while crack slip is associated mainly

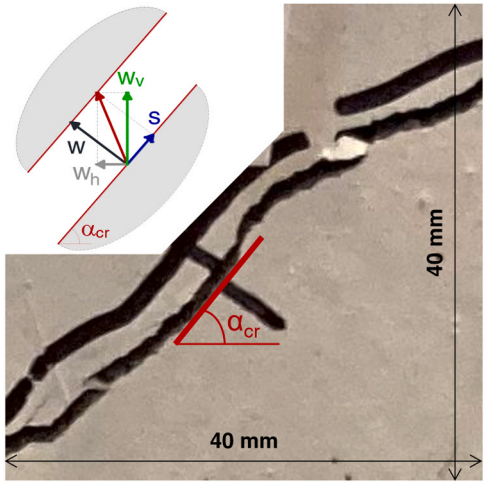

Fig. 2. Definition of crack width w, crack slip s, crack angle α_{cr} and vertical crack displacement w_v.

with shear distortions. Fig. 2 also shows the vertical crack displacement w_v. It can be seen that, within a 40 mm × 40 mm window, in some places the crack surfaces are almost touching while in others they are wide. This illustrates the difficulty of measuring crack widths as it can be challenging to interpret where and how to take the measurements, even along small crack segments.

The crack displacements in specimen CCR2 were also measured using a full view three-dimensional digital image correlation (DIC) system. The crack was discretized in a series of straight segments with a length of approximately one maximum aggregate size a_g, or 19 mm, as recommended by Trandafir et al. [16,17]. This discretization is consistent with the constitutive relationship which will be used later to model aggregate interlock behavior across the cracks. A similar crack discretization approach has been employed by others for the analysis of lab tests of slender beams [18,19]. The crack width w and crack slip s for each segment were obtained from the DIC data as described by Palipana and Proestos [8,9]. Eq. 1 describes how the vertical crack displacements are mathematically related to the crack width and crack slip:

$$w_{v,i} = w_i \cos\alpha_{cr,i} + s_i \sin\alpha_{cr,i} \quad (1)$$

where $\alpha_{cr,i}$ is the local angle of the crack (see Fig. 2). Other DIC data processing tools can also be used to extract w, s, and α_{cr}, such as the automated crack detection and measurement tool (ACDM) developed by Gehri et al. [20]. In field studies where DIC is not available, these quantities can be measured based on image analysis as proposed by Pantoja-Rosero et al. [15].

The variation of crack displacements w, s, and w_v along the critical diagonal crack of specimen CCR2 is shown in Fig. 3 at seven load levels: 40 %, 50 %, 60 %, 70 %, 80 %, 90 % and 100 % of the peak load. Overall, the widths increase from the tip of the crack (loading zone) in the top 2/3 of the beam, and then decrease significantly in the bottom 1/3, near the support (Fig. 3a). More precisely, this measured profile can be divided into three regions: 1) a top region in the vicinity of the loading plate where w increases rapidly away from the tip of the crack; 2) a short middle region characterized by a slower w increase; and 3) a bottom region associated with crack control. The crack control in region 3 is provided by the flexural reinforcement, which forces a series of narrow cracks rather than a single dominant crack (Fig. 1b). It can be seen from Fig. 3a that the maximum crack width measured along the critical crack reached 4.7 mm at failure. Fig. 3a illustrates that in all three regions the crack widths vary significantly. It is important to note that in the second region, the crack widths vary even for adjacent crack segments as also observed in Fig. 2. The variation increased with increasing load and reached ~0.9 mm in region 2 at failure. This raises

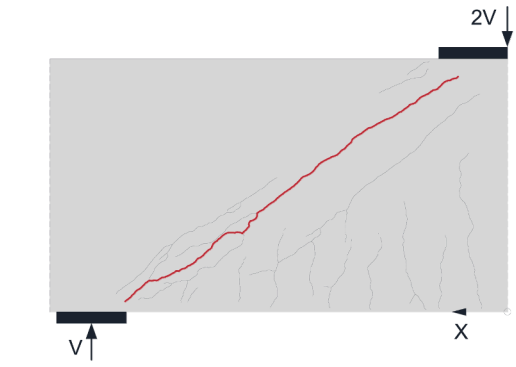

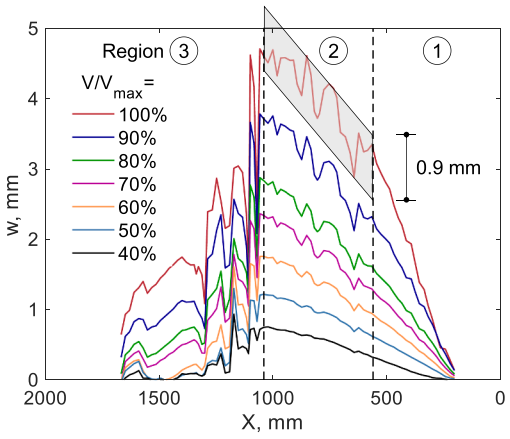

a) Measured crack width profiles

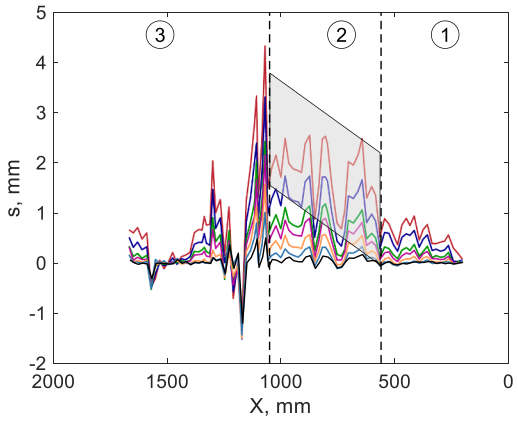

b) Measured crack slip profiles

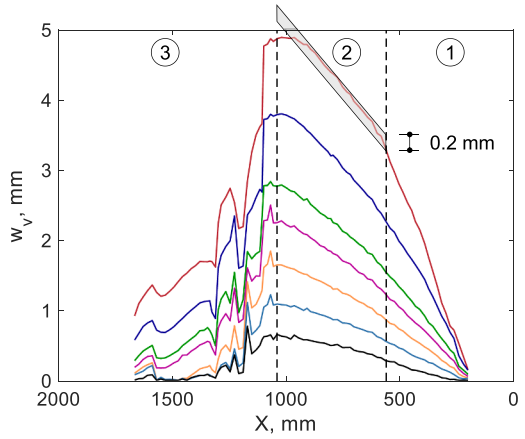

c) Measured vertical crack displacement profiles

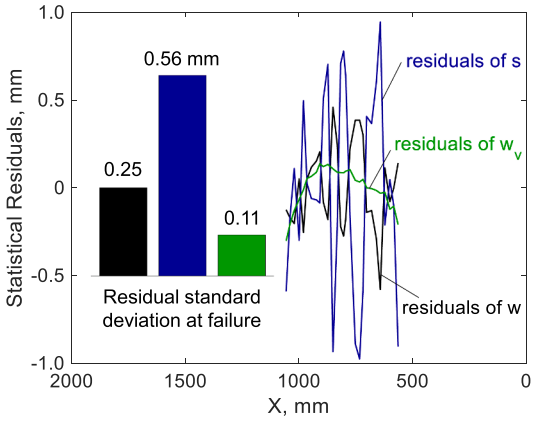

d) Statistical residuals in region 2 at failure

Fig. 3. Measured crack displacement profiles of test specimen CCR2 at 7 load stages: a) crack width; b) crack slip; c) vertical crack displacement; and d) statistical residuals of measurements in region 2 at failure.

the question: Are crack widths the most appropriate measurement for crack-based assessment of deep beams?

Compared to crack widths, the slip displacements show even larger variability from crack segment to crack segment (Fig. 3b). In certain locations along the crack, negative slips are measured when the local crack angle $\alpha_{cr,i}$ is very small. At failure, the crack slip reached values of up to 4.3 mm, which indicates significant shear distortions as is characteristic of deep beams.

Finally, Fig. 3c shows the profile of vertical crack displacements w_v. The same three regions as observed in the crack widths are also observed in the vertical crack displacements (near the tip of the crack, in the region near mid-depth, and in the crack control region). It is immediately apparent that the vertical crack displacements are characterized by a very smooth variation within regions 1 and 2. This is valid for all load levels, from the formation of the critical diagonal cracks to the failure of the member. The maximum value of w_v at failure is 4.9 mm. As indicated in Fig. 3c, the local variation in region 2 is only ~0.2 mm, which is negligible compared to the variations in w and s.

These observations are reinforced in Fig. 3d, which shows the statistical residuals of the three sets of measurements in region 2 at failure. The residuals are defined as the difference between the measured values and linear regressions of the w, s, and w_v profiles. It can be seen that the w_v profile has the least fitting deviation among the three crack measurements, with a residual standard deviation of only 0.11 mm, one-half

of the standard deviation of w.

To conduct crack-based assessments, it is useful if the input parameters do not vary significantly in a particular region. This can help improve field procedures and guidelines for inspectors. Therefore, the negligible local and global variation of w_v in region 2 represents a significant advantage from the point of view of crack-based assessment. The vertical crack displacement in region 1 grow rapidly from zero at the crack tip. The vertical crack displacement in region 3 has significant local variability because of the presence of multiple cracks in that region. Region 2 is located away from the tip of crack and disturbances introduced by the flexural reinforcement in region 3, and therefore is well suited for crack-based assessment. Equally as important, it will be shown later with the help of the two-parameter kinematic theory (2PKT) that w_v is the most suitable indicator of shear failures in deep beams. Therefore, the crack-based assessment method presented in the rest of this paper is based exclusively on measured vertical crack displacements w_v in region 2. The boundaries of this region will also be defined with the help of the 2PKT. This represents a shift of thinking as compared to traditional inspection methods based on crack widths.

3. The crack-based assessment method

In the context of this paper, the assessment of reinforced concrete deep beams is defined as the determination of the remaining capacity a member has to resist shear forces. When this determination occurs by directly using crack information as an input, the method is called a crack-based assessment method. Thus, the crack-based assessment of a deep beam can be represented by plotting the vertical crack displacement w_v on the horizontal axis, and the residual shear capacity on the vertical axis.

Fig. 4 shows how the residual strength of specimen CCR2 decreases with increasing w_v measured at two different locations. The green curve corresponds to $w_{v,top}$ at the top of region 2 (X ≈ 560 mm in Fig. 3c), while the black curve is obtained with $w_{v,bot}$ at the bottom of region 2 (X ≈ 1040 mm in Fig. 3c). The residual strength is defined either in kN as V_{res}= (V_{max}-V), or as a percent $\Psi = 100 \times (1\text{-}V/V_{max})$, where V is the shear force when the crack measurements occur and V_{max} is the peak shear resistance of the member.

In a previous study, Trandafir et al. [16,17] demonstrated the sensitivity of residual shear capacity of deep beams to the specific shape of the critical shear crack. It was illustrated that accounting for crack shape greatly improves the ability to predict deep beam shear response. Therefore, to generate the residual shear capacity versus vertical crack displacement diagrams, it is important to use a modelling framework which incorporates measured crack shapes. In deep beams the critical cracks typically develop at service conditions and therefore can be measured and mapped. Thus, both measuring the vertical crack displacements and crack shape for input into a crack-based assessment model is the goal of this study.

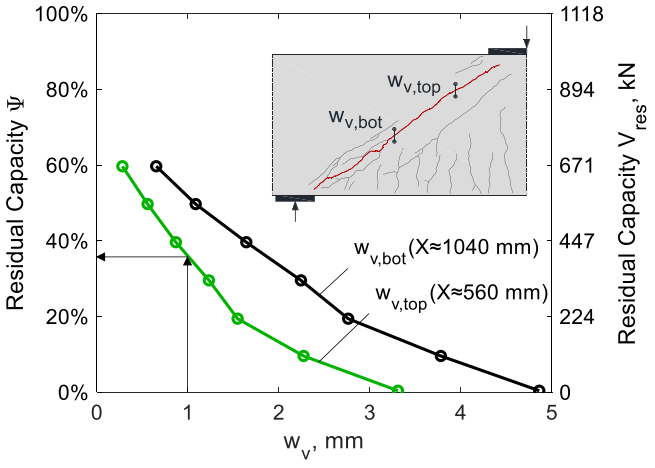

Fig. 4. Measured residual capacity of beam CCR2 as a function of measured vertical crack displacements at two locations.

The modelling framework to accomplish this is the two-parameter kinematic theory (2PKT) [10]. This framework is explicitly based on the kinematics of the critical cracks and can incorporate observed crack shapes. When crack shapes are incorporated in the response predictions, the methodology is called the crack-based 2PKT [16,17]. Thus, the crack-based 2PKT will be used to obtain the V_{res}-w_v and Ψ-w_v diagrams as shown in Fig. 4. With these diagrams an assessment of residual capacity can be directly determined with the measured vertical crack displacements. For example, in the case of specimen CCR2, a measured $w_{v,top}$ of 1 mm should correspond to a residual strength of approximately 400 kN, or 36 %.

4. Formulation of the crack-based 2PKT

4.1. Kinematics of deep beams

The crack-based assessment framework proposed by Trandafir et al. [16,17] is based on the two-parameter kinematic theory (2PKT) [10]. The 2PKT uses two degrees of freedom (DOFs) to model the complete shear behaviour of diagonally cracked deep beams, including local deformations along the critical diagonal cracks. The global kinematics of the model are obtained by superimposing two deformation patterns, and are sufficient to describe the complete deformed shape of a shear span under single curvature – see Fig. 5. The first deformation pattern describes flexural deformations and the second describes shear deformations. The first pattern depends on the average strain along the flexural reinforcement, DOF $\varepsilon_{t,avg}$, and the second pattern is described by the vertical displacement along the critical diagonal crack in the vicinity of the load, DOF Δ_c. The concrete block above the critical crack is modelled as rigid, except for the critical loading zone (CLZ) where the concrete crushes at failure. It is the deformations in the CLZ that give rise

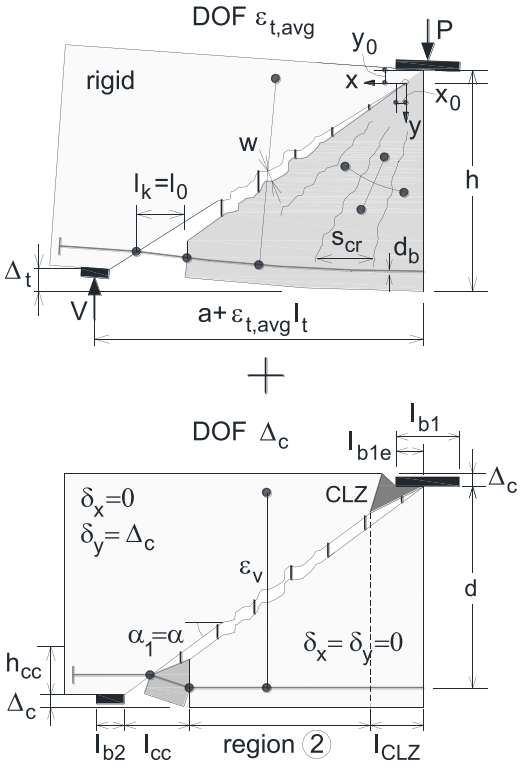

Fig. 5. Two-parameter kinematic theory for deep beams [10].

to DOF Δ_c.

In the crack-based framework, the shape of the critical crack is measured from images. As mentioned earlier, the crack is discretized into straight segments with a length of approximately one maximum aggregate size a_g.

4.2. Crack kinematics

The beam kinematics illustrated in Fig. 5 is consistent with the measured profiles of crack displacements in specimen CCR2. Region 1 in CCR2 corresponds to the CLZ in the 2PKT, where the vertical crack displacements w_v increase linearly away from the loading point. Region 2 in CCR2 corresponds to the middle portion of the crack in the 2PKT, where w_v also increases linearly away from the load, but at a smaller rate. Finally, region 3 in the CCR2 is the region in the vicinity of the bottom flexural reinforcement (tie) in the 2PKT, where w_v decreases approaching the edge of the support. The length of region 1 along the axis of the beam is denoted as l_{CLZ}, while the length of region 3 is l_{cc}.

Based on these kinematics, the vertical displacements of the i^{th} crack segment along the critical crack are expressed with the two DOFs of the kinematic model as follows:

- If $x_i < l_{CLZ}$ (region 1)

$$w_{v,i} = \frac{\varepsilon_{t,avg} l_k}{d - y_0} x_i + \frac{\Delta_c}{l_{clz}} x_i$$

- If $l_{CLZ} \le x_i < a_{cl} + x_0 - l_{cc}$ (region 2)

$$w_{v,i} = \frac{\varepsilon_{t,avg} l_k}{d - y_0} x_i + \Delta_c$$

- If $x_i \ge a_{cl} + x_0 - l_{cc}$ (region 3)

$$w_{v,i} = \left[\frac{\varepsilon_{t,avg} l_k}{d - y_0}(a_{cl} + x_0 - l_{cc}) + \Delta_c\right] \frac{(a_{cl} + x_0 - x_i)}{l_{cc}} \tag{2}$$

where x_i is the horizontal coordinate of the i^{th} crack segment (Fig. 5), a_{cl} is the clear shear span of the beam, and d is the effective depth. Dimensions x_0 and y_0 define the location of the center of rotation in the flexural deformation pattern in Fig. 5, as well as the origin of the x-y coordinate system. Length l_k defines the portion of the flexural reinforcement that contributes to the crack displacements, and is estimated as [10]:

$$l_k = 1.5(h - d)\frac{a_{cl} + l_{b1e}}{h} \ge s_{cr}$$

$$s_{cr} = \frac{0.28 d_b}{\rho_l} \frac{2.5(h - d)}{d} \tag{3}$$

where h is the depth of the beam, d_b is the diameter of the bottom flexural reinforcement, and ρ_l is the ratio of the flexural reinforcement.

Similarly, the horizontal crack displacements can be expressed from the kinematic model as:

- If $x_i < a_{cl} + x_0 - l_{cc}$ (regions 1 and 2)

$$w_{h,i} = \frac{\varepsilon_{t,avg} l_k}{d - y_0} y_i$$

- If $x_i \ge a_{cl} + x_0 - l_{cc}$ (region 3)

$$w_h = \frac{\varepsilon_{t,avg} l_k}{d - y_0}(h - y_0 - h_{cc})\frac{h - y_0 - y_i}{h_{cc}} \tag{4}$$

where y_i is the vertical coordinate of the i^{th} crack segment, and h_{cc} is the depth of region 3. The determination of quantities l_{CLZ}, l_{cc}, h_{cc}, x_0 and y_0 is discussed in the next subsection.

Once w_v and w_h are expressed with DOFs $\varepsilon_{t,avg}$ and Δ_c, they can be used to calculate the corresponding crack width and crack slip for any i^{th} crack segment:

$$w_i = w_{v,i}\cos\alpha_{cr,i} + w_{h,i}\sin\alpha_{cr,i}$$

$$s_i = w_{v,i}\sin\alpha_{cr,i} - w_{h,i}\cos\alpha_{cr,i} \tag{5}$$

The crack widths w and crack slips s determined from these equations are illustrated in Fig. 6 for specimen CCR2. For this illustration, the values of DOFs $\varepsilon_{t,avg}$ and Δ_c were taken to be 1.8×10^{-3} and 3.3 mm, respectively (these values will be discussed further below). The shape of the critical crack was measured and discretized as previously described. It can be seen that the vertical crack displacements follow a tri-linear distribution along the x axis, while the horizontal displacements follow a bi-linear variation. Fig. 6 also shows that the predicted crack widths and slips show significant local variations as observed in the test. The negative term in Eq. 5 also explains why negative slips are sometimes measured on flat crack segments, and can be observed in the predictions and experiments.

4.3. Determination of l_{CLZ}, l_{cc}, h_{cc}, x_0 and y_0 based on measured crack geometry

Since the goal is to perform detailed crack-based assessment, quantities l_{CLZ}, l_{cc}, h_{cc}, x_0 and y_0 are determined based on the measured shape of the critical crack. This will allow to minimize uncertainties in the 2PKT assessments associated with random variations in the paths of the cracks.

To determine the geometry of the CLZ, Trandafir et al. [16,17] have proposed the method illustrated in Fig. 7 (left). Two independent parameters are used to define the geometry: depth d_{CLZ} and the local inclination of the critical crack α_{CLZ}. Depth d_{CLZ} is the shortest distance measured from the edge of the loading plate to the critical crack. To determine the angle α_{CLZ}, a circle is drawn with radius $3d_{CLZ}$, centered at the bottom of the d_{CLZ} length, as shown in Fig. 7 (left). A line is then drawn from the center of the circle to the point where the circle intersects the critical crack. The angle that this line-radius makes with the horizontal is defined as α_{CLZ}. In addition, the center of the circle in Fig. 7 (left) defines the center of rotation of the rigid block x_0 and y_0 used in the derivation of Eqs. 2 and 4.

With the measured d_{CLZ} and α_{CLZ}, the critical loading zone is idealized as triangular region as illustrated in Fig. 7 (right) [10]. The length of

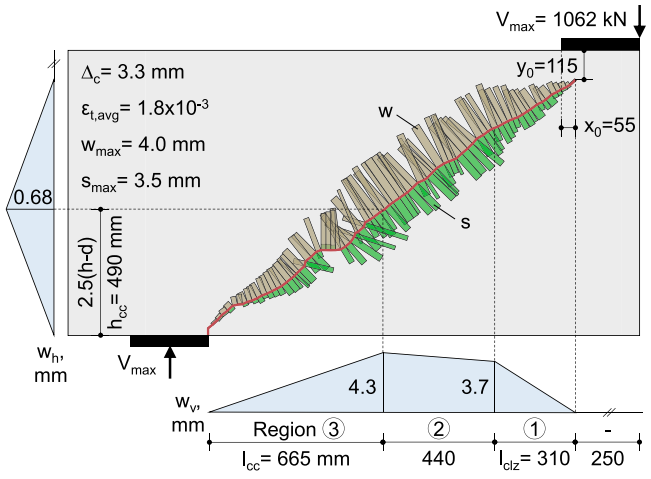

Fig. 6. Predicted crack displacements along the critical diagonal crack of specimen CCR2 at failure.

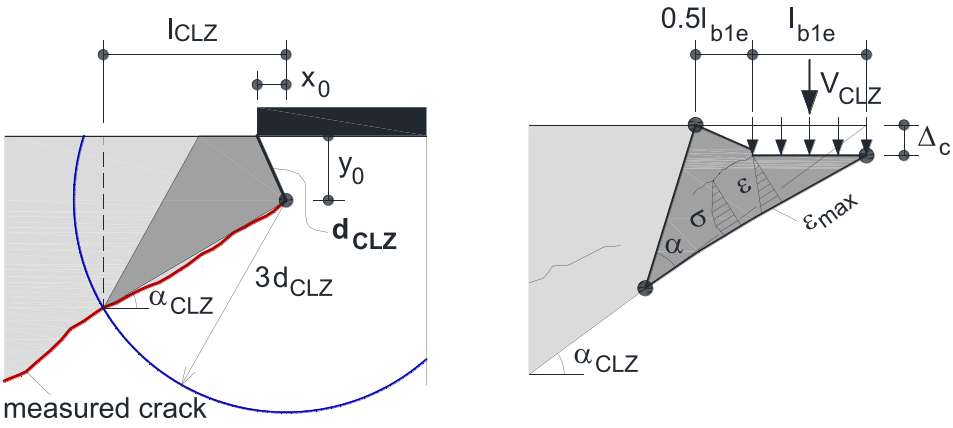

Fig. 7. Crack-based (left) and idealized (right) geometry of the CLZ used in the 2PKT.

the CLZ along the loading plate, l_{b1e}, as well as the length of region 1, l_{CLZ}, are calculated as shown in Eq. 6.

$$l_{b1e} = d_{CLZ}/\sin\alpha_{CLZ}$$

$$l_{CLZ} = 2l_{b1e}\cos^2\alpha_{CLZ} \tag{6}$$

The location of the center of rotation is obtained from:

$$x_0 = l_{b1e}\sin^2\alpha_{CLZ}$$

$$y_0 = l_{b1e}\sin\alpha_{CLZ}\cos\alpha_{CLZ} \tag{7}$$

Note that in the original 2PKT method, the center of rotation is assumed at the center of the loading plate [10]. This is a reasonable assumption for members with relatively small loading plates, where the critical crack typically propagates towards the center of the plate. The approach proposed here is more general, as it also addresses cases of large loading elements, where the crack tip may be closer to the edge of the loading element.

A simpler approach is followed to determine the size of the crack-control region, region 3, in the bottom of the beam. The depth of this region is estimated at h_{cc}=min[2.5(h-d), h/2] based on Eurocode 2 [21]. In a second step, the length of the crack control region l_{cc} is determined as the horizontal projection of the portion of the diagonal crack located within depth h_{cc} (Fig. 6).

4.4. Components of shear resistance

Deep beams carry shear mainly by four mechanisms. These mechanisms include the inclined compression in the CLZ, V_{CLZ}, the aggregate interlock across the crack, V_{ci}, the tension in the transverse reinforcement, V_s, and the dowel action of the bottom flexural reinforcement, V_d. To evaluate shear components V_{CLZ}, V_{ci}, V_s, and V_d, it is necessary to use appropriate constitutive relationships as functions of the two DOFs of the 2PKT, as well as crack displacements w, s, and w_v from Eqs. 2–5. Such relationships have been proposed elsewhere [10,16,17], and are summarized below for the sake of completeness.

4.4.1. Critical loading zone

The idealized CLZ is shown in Fig. 7 (right) and its shear resistance is:

$$V_{CLZ} = \sigma_{avg} b l_{b1e}\sin^2\alpha_{CLZ}$$

$$\sigma_{avg} = \frac{\int_0^{\varepsilon_{max}} \sigma_c(\varepsilon_c)d\varepsilon}{\varepsilon_{max}}$$

$$\varepsilon_{max} = \frac{\Delta_c}{3l_{b1e}\cot\alpha_{CLZ}} \tag{8}$$

where σ_{avg} is the average compressive stress in the CLZ, σ_c=f(ε_c) is the stress-strain relationship of concrete in uniaxial compression [22], ε_{max} is the maximum strain in the CLZ, b is the width of the beam, l_{b1e} is the length of the CLZ along the loading plate, and α_{CLZ} is the angle of the critical crack within the CLZ. Note that l_{b1e} and α_{CLZ} are obtained from the measured crack shape as discussed above. Note also that, globally, the behaviour of the CLZ is expressed with only one of the DOFs of the 2PKT, namely Δ_c.

Using the measured geometry of the CLZ is a key feature of the proposed crack-based approach. As it will be illustrated later, the inclined compression in the CLZ is the dominant mechanism of shear resistance in deep beams, whose failure typically triggers the failure of the beam. At the same time, random variations in the path of the critical crack in the vicinity of the load can significantly alter the capacity of the CLZ, and thus the capacity of the beam [16]. By using the measured l_{b1e} and α_{CLZ}, the crack-based 2PKT directly captures these random effects.

4.4.2. Aggregate interlock

As discussed earlier, the critical diagonal crack is discretized into a series of straight segments. Aggregate interlock stresses are computed on each segment, and are integrated to obtain the shear force carried by this mechanism:

$$V_{ci} = b\left(\sum_i^n v_{ci,i}\sin\alpha_{cr,i}l_i - \sum_i^n n_{ci,i}\cos\alpha_{cr,i}l_i\right)$$

$$v_{ci,i} = 0.35 \bullet 0.635\int_{-\frac{\pi}{2}}^{\frac{\pi}{2}} \sigma_{con}K\sin\theta\cos\theta d\theta (MPa)$$

$$n_{ci,i} = 0.35 \bullet 0.635\int_{-\frac{\pi}{2}}^{\frac{\pi}{2}} \sigma_{con}K\cos^2\theta d\theta (MPa)$$

$$\sigma_{con} = 13.7\sqrt[3]{f_c}\frac{s_i\sin\theta - w_i\cos\theta}{0.04}\begin{cases}\leq 13.7\sqrt[3]{f_c}\\ \geq 0\end{cases}$$

$$K = 1 - \exp\left(1 - \frac{0.5a_g}{w_i}\right) \geq 0 \tag{9}$$

where $v_{ci,i}$ is the shear stress on the i^{th} crack segment, $n_{ci,i}$ is the corresponding normal compressive stress, $\alpha_{cr,i}$ is the angle of inclination of the segment, l_i is the length of the segment, and n is the number of crack segments. The aggregate interlock stresses are obtained from the crack width w_i and crack slip s_i on each crack segment, using the contact density model (CDM) [23] as modified by Trandafir et al. [16]. Note that V_{ci} depends on both DOFs of the kinematic model $\varepsilon_{t,avg}$ and Δ_c via w_i and s_i, through Eqs. 2–5.

Fig. 8 shows the results from these calculations along the critical crack of specimen CCR2. The aggregate interlock stresses correspond to the crack widths and slips in Fig. 6. It can be seen that v_{ci} and n_{ci} vary significantly along the crack with the maximum values occurring on the steepest crack segments. The reason for this result is that the steepest segments feature the smallest crack widths and the largest slip displacements, and thus act as strong shear keys. Therefore, by directly using the measured crack shape, the assessment method is able to capture these local variations of aggregate interlock stresses that influence the shear behavior.

4.4.3. Transverse reinforcement (stirrups)

The stresses and forces in the transverse reinforcement are evaluated individually for each stirrup, and are summed to obtain shear resistance component V_s. All transverse reinforcement crossing the critical crack are taken into account:

$$V_s = \sum_{j}^{m} A_{v,j}\sigma_{v,j} \tag{10}$$

where $A_{v,j}$ is the area of the j^{th} bar, $\sigma_{v,j}$ is the corresponding stress in the bar at the critical crack, and m is the number of bars. Stress $\sigma_{v,j}$ is calculated from the vertical crack displacement at the location of the stirrup $w_{v,j}$ using the pullout model proposed by Sigrist [24]:

$$w_{v,j} = \left(\varepsilon_{v,j} + \frac{f_{yv}}{E_s}\right)L_1 + \min\left(\varepsilon_{v,j}, \frac{f_{yv}}{E_s}\right)L_2$$

$$L_1 = \max\left(\sigma_{v,j} - f_{yv}, 0\right)\frac{d_{bv}}{4f_{ct}}$$

$$L_2 = \min\left(\sigma_{v,j}, f_{yv}\right)\frac{d_{bv}}{8f_{ct}} \tag{11}$$

where f_{yv} is the yield strength of the bars, d_{bv} is the bar diameter, E_s is the modulus of elasticity of the steel, and $f_{ct} \approx 0.26 f_c^{2/3}$ (MPa) is the tensile strength of the concrete. Eq. 11 is solved iteratively by varying the strain in the stirrup $\varepsilon_{v,j}$. For each strain value, the corresponding stress in the stirrup $\sigma_{v,j}$ is calculated from a bi-linear stress-strain relationship for the steel (i.e., elastic-plastic with strain hardening). This approach captures the concentration of stresses in the stirrups in the critical crack. Note that V_s depends on both DOFs of the kinematic model $\varepsilon_{t,avg}$ and Δ_c via crack displacement $w_{v,j}$, through Eq. 2.

4.4.4. Dowel action

The bottom flexural reinforcement is assumed to deform in double curvature over length l_k, and therefore resists shear forces by dowel action:

$$V_d = n_b \frac{12E_s\pi d_b^4}{64 l_k^3}\Delta_c \le n_b f_y \frac{d_b^3}{3l_k}\max\left\{\left[1 - \left(\frac{\varepsilon_{t,avg}}{\varepsilon_y}\right)^2\right], 0\right\} \tag{12}$$

where n_b is the number of bars, d_b is the bar diameter, f_y is the yield stress, and $\varepsilon_y = f_y/E_s$ is the corresponding yield stress. Note that V_d depends on both DOFs of the kinematic model $\varepsilon_{t,avg}$ and Δ_c. Note also that all shear mechanisms depend on the degrees of freedom in a complex nonlinear manner, which does not allow to separate the influence of each DOF on the shear resistance.

4.5. Equilibrium conditions and solution procedure

The crack-based assessment starts by mapping and discretizing the shape of the critical diagonal crack into a series of straight segments. This measured crack shape is then used to determine quantities l_{b1e}, l_{CLZ}, l_{cc}, h_{cc}, x_0 and y_0 as described above. The solution proceeds for a selected value of DOF Δ_c according to the following steps:

1. Select Δ_c;
2. Assume a value of DOF $\varepsilon_{t,avg}$ (e.g., 1.5 $\times 10^{-3}$);
3. Calculate crack displacements $w_{v,i}$, w_i and s_i from Eqs. 2–5;
4. Calculate shear components V_{CLZ}, V_{ci}, V_s, and V_d from Eqs. 8, 9, 10, 11 and 12, respectively;
5. Compare the total shear $V_{CLZ} + V_{ci} + V_s + V_d$ to the shear obtained from the tension of the flexural reinforcement based on moment equilibrium of the shear span:

$$V \approx \frac{E_s A_s \varepsilon_{t,avg}}{a}(0.9d) \tag{13}$$

where A_s is the area of the bottom flexural reinforcement and a is the length of the shear span. Eq. 13 expresses the moment equilibrium taken about the loading point, and is derived from the free-body diagram shown in Fig. 9 (top-right). This expression can also include the tension stiffening effect of the reinforcement within h_{cc} as described elsewhere [16].

- If the two shear forces are not equal (i.e., equilibrium is not satisfied), return to Step 2, and adjust DOF $\varepsilon_{t,avg}$;
- If the shear forces are equal, equilibrium is achieved and the solution at the selected value of Δ_c is complete.

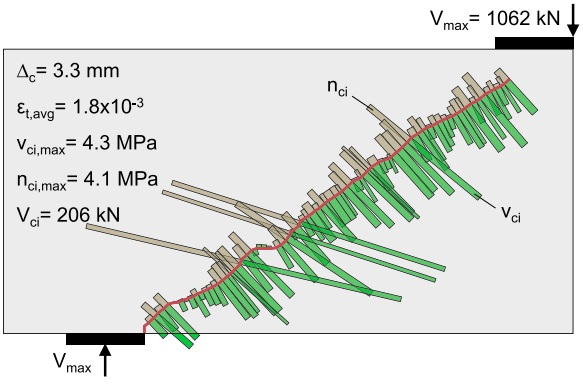

Fig. 8. Predicted aggregate interlock stresses along the critical diagonal crack of specimen CCR2 at failure.

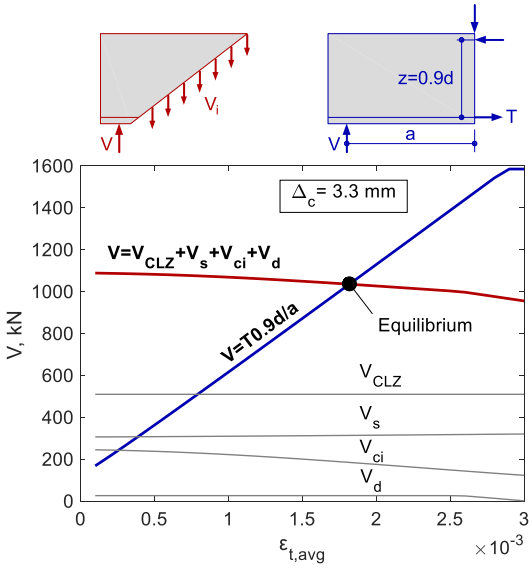

Fig. 9. Equilibrium conditions and solution procedure illustrated for specimen CCR2 at predicted peak load.

This solution procedure is illustrated in Fig. 9 for beam CCR2, where the selected Δ_c value corresponds to the predicted peak response of the beam. In this plot, curve $V=V_{CLZ}+V_{ci}+V_s+V_d$ represents the sum of the four shear-resisting mechanisms along the critical crack, and $V= T(0.9d)/a$ is the shear derived from the moment equilibrium of the shear span (T is the tension in the flexural reinforcement $E_sA_s\varepsilon_{t,avg}$). The solution of the 2PKT equations lies at the point of intersection of the two curves, which is found iteratively. When the calculations are repeated for different values of Δ_c, the complete response of the beam can be obtained, including the pre- and post-peak regimes.

5. Predicted degrees of freedom of specimen CCR2

5.1. DOF $\varepsilon_{t,avg}$

The proposed crack-based approach is first applied to test specimen CCR2. Fig. 10 compares the predicted and measured shear force versus $\varepsilon_{t,avg}$ response of this beam, where the measured values of DOF $\varepsilon_{t,avg}$ are obtained from the DIC data. More precisely, $\varepsilon_{t,avg}$ is equal to the relative horizontal displacement between the centers of the two beam supports, divided by the distance between the supports (span). It can be seen from the figure that the crack-based 2PKT captures well the measured response. The simulation takes into account the tension stiffening effect of the reinforcement, which allows to predict well the measured cracked stiffness. The flexural reinforcement remained in the elastic range up to shear failure. For comparison, Fig. 10 also shows the elastic stiffness assuming a linear variation of longitudinal strain along the span, which agrees well with the experimental response. The cracked elastic stiffness calculated assuming a constant strain along the longitudinal reinforcement is also shown; however, it does not predict the response of the member well. The crack-based assessment approach, while making simplifying assumptions in the uncracked regime, captures the response of the member well throughout loading.

5.2. DOF Δ_c

Fig. 11 shows the measured and predicted response of specimen CCR2 in terms of shear force versus DOF Δ_c. While DOF $\varepsilon_{t,avg}$ could be measured directly, Δ_c can only be estimated from the DIC data. According to the kinematic model in Fig. 6, Δ_c can be estimated from the measured vertical crack displacements w_v. In particular, w_v near the load is dominated by Δ_c, while the contribution of $\varepsilon_{t,avg}$ is limited. Therefore, it is proposed to estimate Δ_c from the DIC data as the vertical crack displacement w_v at $x = l_{CLZ}$. In other words, according to Fig. 3c, Δ_c is equal to w_v at the boundary between regions 1 and 2. Note that l_{CLZ} is obtained from the measured crack shape as discussed earlier, and equals

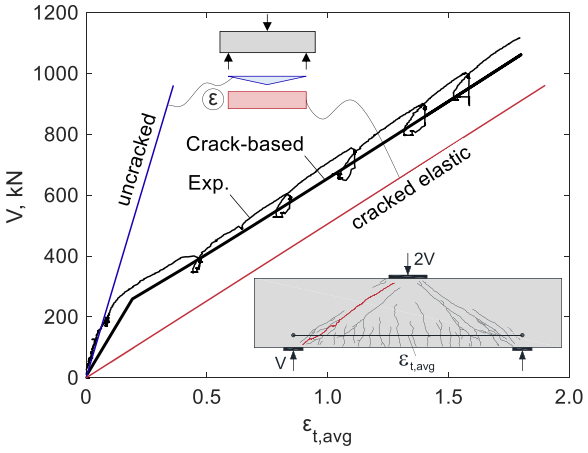

Fig. 10. Behaviour of the longitudinal reinforcement.

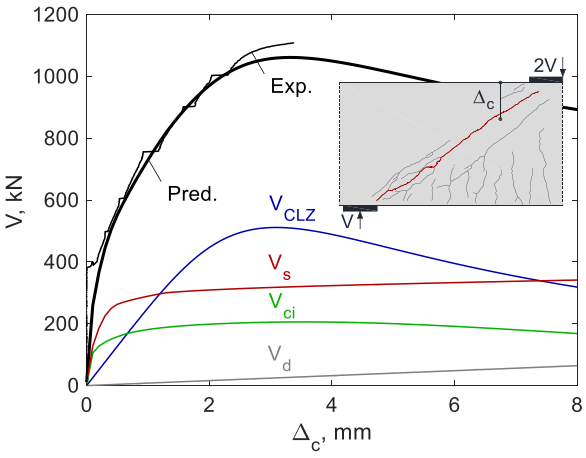

Fig. 11. Behaviour of the critical loading zone.

310 mm for specimen CCR2.

It can be seen from Fig. 11 that the crack-based 2PKT captures well the complete V-Δ_c response of beam CCR2 from the first cracking until failure. The shear strength experimental-to-predicted ratio is 1118/1062 = 1.05. The plot also shows the predicted shear components V_{CLZ}, V_{ci}, V_s, and V_d as they vary with increasing Δ_c. The dominant mechanism for this beam is the inclined compression in the critical loading zone, V_{CLZ}, which accounts for 48 % of the peak resistance. The second most important strength contribution is provided by the stirrups V_s, accounting for 30 %, while the aggregate interlock V_{ci} accounts for 19 % of the shear strength. The evaluation of V_{ci} is illustrated in Fig. 6 and Fig. 8, where DOFs $\varepsilon_{t,avg}= 1.8 \times 10^{-3}$ and $\Delta_c= 3.3$ mm correspond to the predicted values at peak load. The remaining contribution of 3 % is due to the dowel action of the bottom reinforcement, V_d. The shear reinforcement is predicted to yield early in the response of the member (see red curve) and the failure is triggered by crushing of the CLZ (blue curve). This is consistent with the test, as the beam was observed to fail in shear with crushing of the concrete near the loading plate (Fig. 1c).

6. Critical crack displacement for crack-based assessment

The comparisons made in Fig. 11 allow to draw an important conclusion regarding the critical crack displacement that needs to be measured in crack-based assessments of deep beams. Earlier, it was concluded that it is necessary to measure the vertical crack displacements w_v in region 2 as they vary smoothly and can be measured reliably. According to the 2PKT, these displacements are also important from a physical point of view, as they relate mostly to the shear deformations in Fig. 6. Furthermore, w_v at $3d_{CLZ}$ from the tip of the crack (the top of region 2) quantifies the deformations of the critical loading zone (CLZ), which typically triggers the failure of deep beams. Therefore, w_v at $x = l_{CLZ}$ is used as the critical assessment parameter. In the 2PKT calculations, this corresponds to DOF Δ_c. Both will be denoted $w_{v,cr}$, the critical vertical crack displacement.

It should be noted that the crack-based 2PKT is able to predict crack displacements along the critical crack, including at the locations of the crack measurements shown in Fig. 3. Therefore, any crack displacement in region 1 and 2 could be used for crack-based assessment. It is just necessary to perform the measurement and prediction for the same point. Nevertheless, the critical vertical crack displacement $w_{v,cr}$ measured in the vicinity of the compression zone is preferred as it directly quantifies the transverse (shear) deformations of the member. In other words, $w_{v,cr}$ is not affected by flexural deformations, which are not strongly linked with the shear distortion, shear strength, and failure mode of deep beams.

7. Residual capacity diagrams obtained with the crack-based 2PKT

7.1. Specimen CCR2

Fig. 12 illustrates the proposed crack-based assessment framework for deep beams, as applied to specimen CCR2. The plot is obtained directly from the data in Fig. 11, except that the left vertical axis is now the residual capacity (Ψ) of the beam in %. The shear strength contributions are plotted on the right vertical axis, which is inverted so that curves V_{CLZ}, V_{ci}, V_s, and V_d follow the residual capacity curve. As can be seen in the figure, the crack-based assessment (solid thick black curve) is in good agreement with the measured response (solid thin black curve). The residual shear resistance of the beam decreases gradually under increasing $w_{v,cr}$ up to failure. For a given measured $w_{v,cr}$, the solid prediction diagram can be used to evaluate the residual load-bearing capacity of the member. For example, if the measured value of $w_{v,cr}$ is 1 mm, the crack-based assessment results in a residual capacity of 30 % for the member under consideration.

Fig. 12 also shows the residual capacity of test specimen CCR2 obtained from the 2PKT in a case when the crack shape is unknown (simplified method – dashed thick black). In this case, a straight crack is assumed as described in detail elsewhere [10,17]. Although the shear strength experimental-to-predicted ratio obtained with the simplified approach remains adequate at 1118/985 = 1.14, this approach produces unconservative predictions of the residual capacity of the beam as a function of $w_{v,cr}$. This comparison shows that the crack-based 2PKT with measured CLZ geometry produces significantly better structural assessment results.

7.2. Residual capacity evaluation of deep beams tested by Mihaylov et al.

Two deep beam tests performed by Mihaylov et al. [1] are also used for the validation of the direct crack-based assessment framework. The two specimens were subjected to three-point bending, and had an a/d ratio of 1.55, an effective depth d= 1095 mm, and a total depth h= 1200 mm. The beams featured a flexural reinforcement ratio of 0.70 %, while the maximum coarse aggregate size was a_g= 20 mm. While specimen S0M had no stirrups, beam S1M had a transverse reinforcement ratio of 0.10 %. The concrete compressive strength of beams S0M and S1M was f_c= 34.2 MPa and 33.0 MPa, respectively. Further details related to the crack-based modelling of the two deep members are provided elsewhere [16].

Mihaylov et al. [1] used an orthogonal grid of Zürich targets to record the deformations of each member of the mesh at each load step. Therefore, pairs of targets can be used to determine discrete crack displacements [1]. However, as the mesh density is much coarser compared to the DIC measurements of beam CCR2, the selection of deformations is limited to targets that are crossed only by the critical crack. This ensures that the deformations are concentrated in the studied critical crack, including negligible concrete strains between targets. To measure the transverse displacement $w_{v,cr}$, a linear interpolation is performed between the point of zero relative vertical crack displacement (that is, approximately the center of the loading plate), and the closest pair of targets outside the CLZ. For beam S0M the closest pair of targets is located at 600 mm measured from beam midspan, while for specimen S1M the pair of interest is positioned at 300 mm.

Fig. 13 shows that the crack-based predicted residual capacity as a function of $w_{v,cr}$ is in good agreement with the measured values for both beams. Fig. 13 (top) also shows the contribution of each load-bearing mechanism in specimen S0M. Note that the shear resistance of this beam was governed by the aggregate interlock mechanism. As illustrated in Fig. 13 (bottom), a different behaviour was exhibited by beam S1M that featured stirrups. The small stirrup ratio was not able to transfer across the critical crack more shear than the aggregate interlock and CLZ components. For beam S1M, the two main strength mechanisms – aggregate interlock and CLZ – carried almost the same amount of load at peak resistance.

7.3. Residual capacity evaluation of a 4-m deep beam test specimen

To further validate the direct crack-based assessment approach, it is proposed to calculate the residual capacity of a unique large-scale deep beam specimen PLS4000W tested to failure by Collins et al. [25] at the University of Toronto. The beam had a total depth of 4 m and a shear-span-to-effective-depth ratio of 1.82. The flexural reinforcement ratio was 0.656 %, while the stirrup ratio was 0.08 %. The compressive

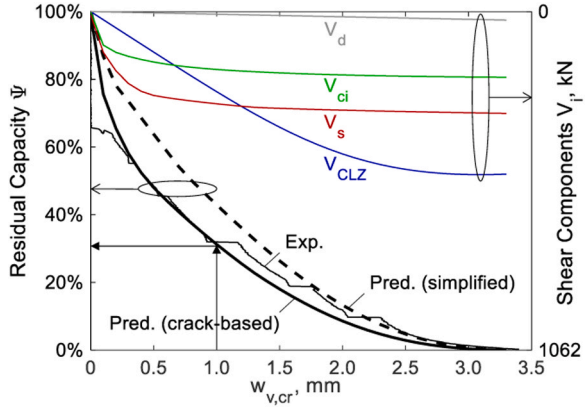

Fig. 12. Measured and predicted residual capacity of specimen CCR: crack-based simulation (solid line) and simplified straight crack simulation (dashed line).

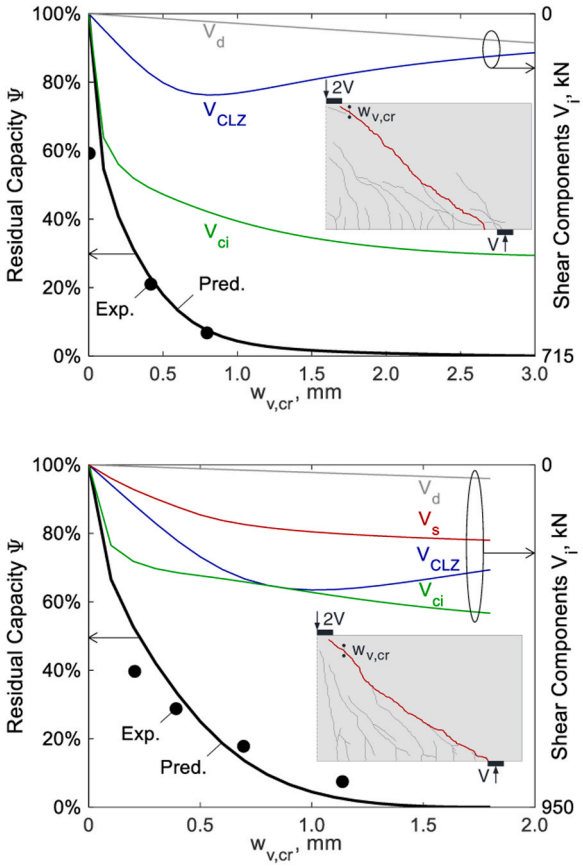

Fig. 13. Measured and predicted residual capacity of specimens S0M (top) and S1M (bottom).

strength of the concrete was f_c= 44.2 MPa and the maximum aggregate size was a_g= 14 mm. The complete load-deflection response of the deep shear span has been previously simulated with the crack-based model, and further details related to the modelling of this member are provided elsewhere [17]. In this paper, the deep shear span of the 4-meter-deep member is exclusively used for the validation of the direct crack-based assessment.

Collins et al. [25] used a vertical displacement transducer to measure deformations in the vicinity of the loading plate. The transducer was installed within the CLZ, at 250 mm measured horizontally from the middle of the loading plate. To determine the measured value of $w_{v,cr}$, it is necessary to extrapolate the reading to the edge of the CLZ.

As shown in Fig. 14, the direct assessment approach that makes use of the crack-based simulation is able to capture accurately the residual capacity of the specimen up to failure. Although the shear reinforcement ratio is relatively low in this member, the largest contribution to the shear resistance is provided by the stirrups.

It is important to note that all studied specimens featured different governing mechanisms of shear resistance. Specimen CCR2 was governed by the critical loading zone, specimen S0M was governed by aggregate interlock, the 4-meter deep Toronto specimen was governed by the transverse reinforcement, and S1M combined significant critical loading zone and aggregate interlock contributions. The results indicate that the assessment method can capture the complete range of these failure mechanisms and the residual capacity for all ranges of $w_{v,cr}$, the critical vertical crack displacement.

7.4. Summary of crack-based assessment results

Table 1 presents a summary of the results using the crack-based assessment approach described in this paper. The table provides a comparison of the measured and predicted peak shear force V_{max}, as well as the two DOFs described in the 2PKT, $\varepsilon_{t,avg}$ and Δ_c. The results indicate that the crack-based assessment approach performs well for all the specimens examined.

8. Summary and conclusions

The paper set out to answer three questions as they relate to the crack-based assessment of lightly reinforced concrete deep beams:

1) Which critical crack displacements should be measured?
2) Where should the critical crack displacements be measured along the cracks?
3) How to assess the residual shear capacity of the member, given the measured critical crack displacements?

The means used to address these questions included a detailed analysis of data from the CCR2 experiment, as well as the modelling framework provided by the 2PKT. The conclusions pertaining to the three questions are the following:

1. The vertical crack displacements are most conducive for crack-based assessments of deep beams. It was illustrated that these displacements vary smoothly along the critical cracks, and therefore do not render the assessment approach sensitive to small variations in measurements. Equally as important, the vertical crack displacements are closely linked to the shear deformations governing the response of deep members. In contrast, crack widths were shown to exhibit rapid variations even along small crack segments.
2. The critical vertical crack displacement is taken in the vicinity of the critical loading zone, where the concrete crushes at failure. The exact location is defined by the size of the critical loading zone which is obtained from the measured crack shape. Closer to the load and near the support the vertical crack displacements are significantly disturbed by the load and flexural reinforcement, respectively.
3. The residual shear capacity of deep members can be assessed using the crack-based 2PKT. The input for assessment includes the measured shape of the critical crack, as well as the measured critical vertical crack displacement. The crack-based assessment method was able to determine the residual capacity of four deep members with variable properties and governing shear carrying mechanisms.

In this crack-based assessment framework, the methodology developed is based on the kinematics of a specific structural typology. An important challenge for the future is to apply these lessons and methods to other structure typologies governed by different kinematics. Similarly, it is necessary to develop an understanding of how these methods can be applied in the field to conduct reliably structural assessments directly from cracks.

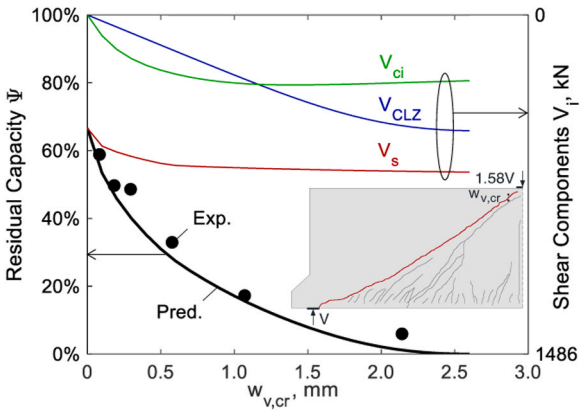

Fig. 14. Measured and predicted residual capacity of the deep shear span of the 4-m-deep Toronto specimen.

Table 1
Summary of crack-based assessment measured and predicted values at failure.

Beam	$\varepsilon_{t,avg} \times 10^{-3}$		Δ_c, mm		V_{max}, kN		V_{exp}/V_{pred}
	Exp.	Pred.	Exp.	Pred.	Exp.	Pred.	
CCR2	1.80	1.79	3.38	3.30	1118	1062	1.05
S0M	2.01	1.65	0.80	0.80	721	715	1.01
S1M	2.18	2.29	1.14	0.90	941	950	0.99
PLS4000W	2.00	2.32	1.80	2.14	1509	1486	1.02

Note: Experimental and predicted Δ_c values near failure at $\Psi = 7$ % for beams S0M, S1M, and PLS4000W.

CRediT authorship contribution statement

Alexandru N. Trandafir: Writing – original draft, Visualization, Validation, Software, Methodology, Conceptualization. **Boyan I. Mihaylov:** Writing – original draft, Visualization, Supervision, Project administration, Methodology, Conceptualization. **Giorgio T. Proestos:** Writing – review & editing, Visualization, Supervision, Funding acquisition, Conceptualization. **Dhanushka K. Palipana:** Investigation, Data curation.

Declaration of Competing Interest

The authors declare that they have no known competing financial interests or personal relationships that could have appeared to influence the work reported in this paper.

Data availability

Data will be made available on request.

Acknowledgements

The research was conducted by the authors as a part of an ongoing international collaborative effort on the Crack-Based Assessment of Concrete Structures (CBACS).

References

[1] Mihaylov BI, Bentz EC, Collins MP. Behavior of large deep beams subjected to monotonic and reversed cyclic shear. Acids Struct J 2010;107(6):726–34.
[2] Aravinthan T, Suntharavadivel TG. Effects of existing shear damage on externally posttensioned repair of bent caps. J Struct Eng 2007;133(11):1662–9.
[3] Birrcher D., Tuchscherer R., Huizinga M., Bayrak O., Wood S.L., Jirsa J.O. Strength and serviceability design of reinforced concrete deep beams. Report No. FHWA/TX-09/0–5253-1, The University of Texas at Austin; 2009.
[4] Larson N., Gomez E.F., Garber D., Bayrak O., Ghannoum W.M. Strength and serviceability design of reinforced concrete inverted-T beams. Report No. FHWA/TX-13/0–6416-1, The University of Texas at Austin; 2013.
[5] Calvi PM, Proestos GT, Ruggiero DM. Towards the development of direct crack-based assessment of structures. Acids Spec Publ 2018;328(9):1–18.
[6] Zaborac J, Athanasiou A, Salamone S, Bayrak O, Hrynyk TD. Crack-based shear strength assessment of reinforced concrete members using a fixed-crack continuum modeling approach. J Struct Eng 2020;146(4):04020024.
[7] Vecchio FJ, Collins MP. The modified compression-field theory for reinforced concrete elements subjected to shear. Acids Struct J 1986;83(2):219–31.
[8] Palipana DK, Proestos GT. Large-scale shear critical reinforced concrete deep beam experiments monitored with full field of view digital image correlation equipment. Trans, SMiRT-26 Berl/Potsdam, Div V, Ger 2022.
[9] Palipana D.K. Assessment of shear transfer mechanisms in reinforced concrete deep beams from experiments with full field-of-view displacement field data [Ph.D. thesis]. North Carolina State University; 2023. Available from: URI: https://www.lib.ncsu.edu/resolver/1840.20/40757.
[10] Mihaylov BI, Bentz EC, Collins MP. Two-parameter kinematic theory for shear behavior of deep beams. Acids Struct J 2013;110(3):447–55.
[11] Li G, Liu Q, Zhao S, Qiao W, Ren X. Automatic crack recognition for concrete bridges using a fully convolutional neural network and naive Bayes data fusion based on a visual detection system. Meas Sci Technol 2020;31(7):075403.
[12] Koch C, Georgieva K, Kasireddy V, Akinci B, Fieguth P. A review on computer vision based defect detection and condition assessment of concrete and asphalt civil infrastructure. Adv Eng Inf 2015;29(2). 196-10.
[13] Kim B, Cho S. Automated vision-based detection of cracks on concrete surfaces using a deep learning technique. Sensors 2018;18(10):3452.
[14] Valença J, Puente I, Júlio ENBS, González-Jorge H, Arias-Sánchez P. Assessment of cracks on concrete bridges using image processing supported by laser scanning survey. Constr Build Mater 2017;146:668–78.
[15] Pantoja-Rosero BG, dos Santos KM, Achanta R, Rezaie A, Beyer K. Determining crack kinematics from imaged crack patterns. Constr Build Mater 2022;343:128054.
[16] Trandafir AN, Palipana DK, Proestos GT, Mihaylov BI. Framework for crack-based assessment of existing lightly-reinforced concrete deep members. Acids Struct J 2022;119(1):255–66.
[17] Trandafir AN, Proestos GT, Mihaylov BI. Detailed crack-based assessment of a 4-m deep beam test specimen. Struct Conc 2023;24(1):756–70.
[18] Campana S, Fernández-Ruiz M, Anastasi A, Muttoni A. Analysis of shear-transfer actions on one-way RC members based on measured cracking pattern and failure kinematics. Mag Conc Res 2013;65(6). 386-04.
[19] Cavagnis F, Fernández-Ruiz M, Muttoni A. An analysis of the shear-transfer actions in reinforced concrete members without transverse reinforcement based on refined experimental measurements. Struct Conc 2018;19(1):49–64.
[20] Gehri N, Mata-Falcón L, Kaufmann W. Automated crack detection and measurement based on digital image correlation. Constr Build Mater 2020;256:119383.
[21] CEN European Committee for Standardization. Eurocode 2. Design of concrete structures Part 1–1: General rules and rules for buildings. Brussels (Belgium): EN 1992–1-1; 2004. p. 225.
[22] Popovics S. A numerical approach to the complete stress-strain curve of concrete. Cem Conc Res 1973;3(5):583–99.
[23] Li B, Maekawa K, Okamura H. Contact density model for stress transfer across cracks in concrete. J Fac Eng, Univ Tokyo 1989;40(1):9–52.
[24] Sigrist V. On the deformation capacity of reinforced concrete girders (German: Zum Verformungsvermögen von Stahlbetonträgern), Diss., IBK, ETH Zürich, Switzerland; 1995.
[25] Collins M.P., Bentz E.C., Quach P.T. Shear behavior of thick slabs. ACI Struct J, 117 (4). p. 115–26.